Exploring the Spatiotemporal Variation of Air Pollution Throughout the Urban Landscape of Philadelphia, PA with Mobile Monitoring

Lucas E. Cummings*[1], Justin D. Stewart*[1,2], Radley Reist[1], Kabindra M. Shakya[1**], Peleg Kremer[1]

**These authors contributed to this work equally*

[1]Department of Geography and the Environment, Villanova University, Pennsylvania, USA

[2]Department of Ecological Science, Vrije Universiteit Amsterdam, 1081 HV Amsterdam, Netherlands

****Corresponding author**

800 Lancaster Avenue, Villanova, PA 19085, USA

Department of Geography & the Environment

Villanova University

Phone: 610-519-3590

Email: kabindra.shakya@villanova.edu

Author Contributions:

Conceptualization: KMS, PK. *Data Collection:* JDS, RR, KMS, PK. *Formal Data Analysis:* JDS, LEC, RR. *Writing:* LEC, JDS, RR, KMS, PK. *Supervision & Funding Acquisition:* KMS, PK

ORCID:

LEC: 0000-0002-7685-0525

JDS: 0000-0002-7812-5095

PK: 0000-0001-6844-5557

KMS: 0000-0002-7035-7019

Sources of Support: NSF Grant # 1832407

Word count: 5755

Abstract

In this study, we implement a mobile monitoring methodology in order to determine the spatiotemporal distribution of particulate matter (PM) and black carbon (BC) in Philadelphia, PA, USA. Over the course of 12 days between June 27, 2019 and July 29, 2019, we measured air pollution concentrations across two replicated 150-mile long routes. Mean concentrations for each pollutant were 11.25 ± 5.43 ug/m^3 (PM_1), 11.08 ± 6.25 ug/m^3 ($PM_{2.5}$), 15.57 ± 8.51 ug/m^3 (PM_{10}), and 1.27 ± 0.80 µg/m^3 (BC). We find that finer PM size fractions ($PM_{2.5}$ and smaller) constitute approximately 71% of PM_{10}. Air pollution hotspots across three size fractions of PM (PM_1, $PM_{2.5}$, and PM_{10}) and BC were present throughout Philadelphia, but were most prevalent in the North Delaware, River Wards, and North planning districts. A plurality of air pollution hotspots found throughout the data collection period (30.19%) occurred between the hours of 8:00 AM – 9:00 AM. Despite significant temporal variation, pollutant concentrations, except for PM_{10}, clustered temporally with a separation before 12 PM. Our approach and findings identify times and places where pollutant concentrations are highest, which is integral to effective air pollution reduction in urban environments.

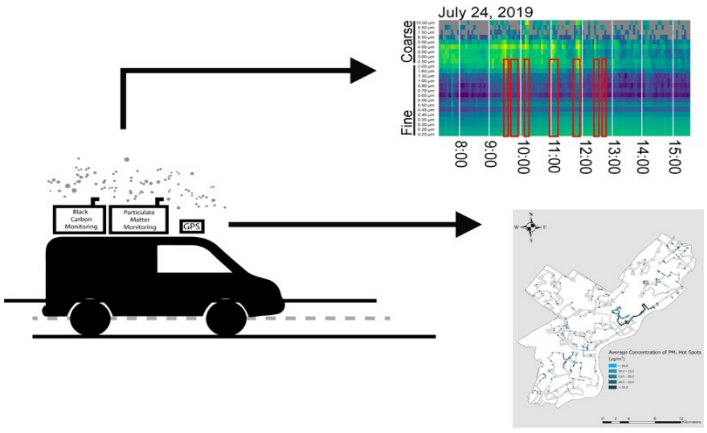

Introduction

Air pollution is a major environmental threat for urban populations, affecting the health of 9 out of 10 urban residents[1]. Within urban environments, locally high concentrations of air pollutants are common[2]. As populations continue to migrate to urban areas[3], we can expect air pollution to continue to present health risks for human populations. In order to attenuate negative health impacts[1] of air pollution in the future, it is imperative that we are able accurately assess the spatiotemporal distribution of air pollution in urban environments. Comprehensive air pollution monitoring is crucial to understanding where and how to focus efforts to attenuate air pollution and its associated health risks in the urban environment.

Particulate matter (PM) consists of heterogeneous mixtures of organic[4] and inorganic components[5] that vary in size, shape, composition, and origin within the urban environment[6]. Coarse size fractions (PM_{10} – $PM_{2.5}$) of PM largely originate from crustal sources, whereas fine PM ($PM_{2.5}$ – $PM_{0.1}$) derive mainly from industrial emissions, non-renewable power generation, and vehicle exhausts[7]. Black carbon (BC) is a major component of PM that results from the incomplete combustion of fossil fuel and other organic matter. As such, the presence of BC is often used as an indicator of urban traffic pollution[8]. Quantifying the abundance and distribution of various PM sizes in urban environments is of particular interest to public health[9], as prolonged exposure to PM is associated with increased rates of mortality[10]; small particles easily deposit in the lungs[11], leading to a number of observed negative health outcomes including reduced lung function[12], asthma[13], cardiovascular and respiratory disease[14], and pathogen exposure[15].

Many studies have investigated urban air quality, but these studies tend to rely on a small number of stationary points of measurement[16,17] and interpolation[18,19] to characterize air pollution across an entire city. While these methods are effective at capturing temporal trends in local pollutant concentrations, they are unable to capture fine-scale spatial variation in air pollution throughout urban environments. In recent years, mobile monitoring has emerged as a novel method with which to study the spatial and temporal distribution of air pollutants[6,20–22]. As mobile monitoring methods are capable of collecting data at finer spatial scales than is feasible with stationary monitoring[6,23], mobile monitoring can provide more accurate information about air quality within the city. In this study, we employ vehicular mobile monitoring of PM across 24 different size fractions between 10 – 0.25 μm and BC throughout the urban landscape of Philadelphia, Pennsylvania and identify statistically significant hotspots of air pollution in time and space during the summer of 2019. With mobile monitoring, we can observe the spatiotemporal distribution of air pollutants and discern patterns in variation at a fine spatial scale. By doing so, it is possible to identify locations in urban environments where high concentrations of air pollutants are common[24] and provide more holistic assessments of risks associated with air pollution in urban areas.

Methods

Site Description:

Philadelphia, Pennsylvania, USA had an estimated population of 1,584,138 in 2018. Located in the Mid-Atlantic region, Philadelphia is dominated by a dense urban center surrounded by predominantly low-rise residential and commercial districts, city parks, and

industrial sectors. The city's eastern border is defined by the Delaware River, which flows southward to the Delaware Bay and Atlantic Ocean, while the city's other major river, the Schuylkill River, flows southward to the Delaware through the western neighborhoods of Philadelphia. The southern and eastern parts of the city house heavy industry along both riverbanks (Planning Districts Lower Southwest, Lower South, and River Wards), while large park areas are found in the western and northern areas of the city (Planning Districts Lower Northwest, Upper Northwest, and Central Northeast) (Figure 1). Philadelphia consistently ranks as one of the most polluted metropolitan areas in the United States[14].

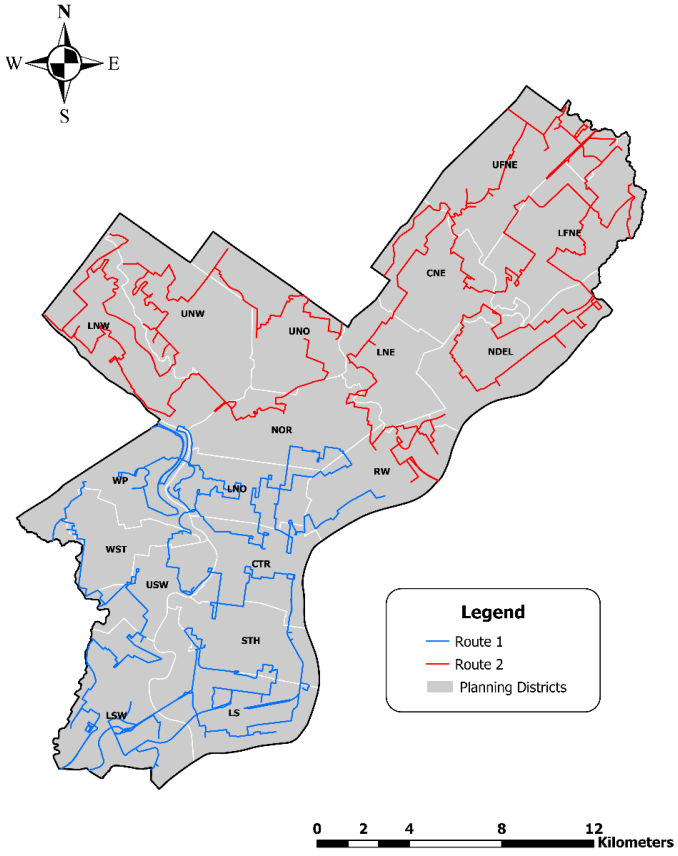

Figure 1. Map of study area, including routes traveled and Philadelphia planning districts.

Sampling Description:

A driving route was developed using a stratified random selection of points representing different combinations of urban structure to provide a representative sample of Philadelphia for mobile monitoring. Additionally, selected points of interest, such as industrial sites, United States Environmental Protection Agency (U.S. EPA) Toxics Release Inventory (TRI) sites, and EPA air pollution monitoring station sites, were included in route development. The optimized driving route, which passed through the selected sample points, was created using ESRI ArcGIS 10.7.1 Network Analyst, and the resulting ~300 mile route was then split into two near-equal segments of approximately 150 miles each, with each segment being drivable in a single day.

A van, equipped with two global positioning system (GPS) units (Trimble Juno 3B fitted with Trimble R1 GNSS receivers) and instrumentation measuring PM (GRIMM Portable Laser Aerosol Spectrometer, Model 11-C) and BC (MicroAeth MA200), was driven along the two predetermined routes in Philadelphia. The GRIMM spectrometer was factory calibrated prior to the monitoring campaign. Air pollution instrumentation was placed inside a box attached to the roof of a van (~1.5 meters), and the inlets of the instrumentation were connected to an isokinetic sampling probe of diameter 1.5 mm. Measurements were conducted over a period of 12 day between June 27, 2019 and July 29, 2019. Measurement would begin between the hours of 6:00 AM and 7:00 AM on one of the two routes and continued until the entirety of the route was travelled. In order to maintain continuous measurements in the face of satellite reception issues and equipment malfunction, the two GPS units were used simultaneously. Occasional road closures in Philadelphia created slight variability in the routes traveled from day to day (SI-1). Data was captured at different temporal resolutions; GPS data was recorded

for every one second interval, while BC data was recorded every five seconds and PM data was recorded every six seconds.

Data Processing/Analysis:

Air pollution and GPS data were joined by time to create a database of geolocated air pollution data. Histograms and quantile-quantile plots were used to remove the top and bottom 0.5% of air pollution measurements. Pollution data lacking geolocation information due to instrument error was not considered for spatial analysis in this paper. One day (July 15, 2019) is entirely excluded from spatial analysis as a result of GPS malfunction that resulted in a significant amount of missing geolocation data. Vector (point) datasets representing air pollution along the routes were created and used for representation and spatial analysis.

Spatial analysis was conducted in ESRI ArcGIS Pro 2.4. Point datasets were projected into the Pennsylvania State Plane South projected coordinate system. Air pollution data was spatially joined to a systematic grid of 120 m^2 fishnet cells overlaid on Philadelphia, which has previously been used to generalize and characterize urban landscape and ecosystem function[6,25,26]. All points falling within a given cell were averaged to determine the average concentration of pollutants in that 120 m^2 area. For each day of data collection, PM_1, $PM_{2.5}$, PM_{10}, and BC hotspots with statistical significance at a 95% confidence level were identified using the Hot Spot Analysis (Getis-Ord Gi*) tool. Hotspot analysis allows for the identification of statistically significant locations in a study area where features with high or low values cluster within the context of its neighborhood[27]. The neighborhood threshold radius for all hotspot analyses was set at the minimum distance to ensure that for each day, observations for all

pollutants measured had at least one other feature designated as a neighbor (615 m). The inverse distance squared conceptualization of spatial relationships was used for this analysis, which sees the influence of an observation on its spatial neighbors decrease significantly with increasing distance. False discovery rate correction was applied to correct for false positives. In order to compare the locations of hotspots across the days of data collection, significant hotspots ($p < 0.05$) for each day were spatially joined with the fishnet grid. Hot spots within a given cell were averaged to determine the mean pollution concentration of the hotspots in each cell for each day. Data for PM and BC concentrations and GPS coordinates for hotspots can be accessed at https://github.com/Shakya-Kremer-Lab/AirPollution.

Statistical analysis was conducted in R (3.6.1). Combination violin and boxplots were produced to show the range and distribution of air pollutants across all days. Pairwise Mann-Whitney tests with Bonferroni correction on mass concentrations for the PM_1, $PM_{2.5}$, PM_{10} size fractions – chosen as representatives of the fine-to-coarse PM size fraction gradient – and BC were conducted to test if pollution levels differed between days. The relationship between BC and $PM_{2.5}$ was tested at the univariate level with Bonferroni corrected Spearman correlations. Multivariate relationships between BC and $PM_{2.5}$ were assessed using permutational (n=999) Procrustes rotations. This test compares a collection of multidimensional shapes by transforming them into a state of maximal superimposition and resulting in a correlation coefficient, m^2.

Temporal variation in mass values for PM across size fractions during core times (where data overlaps on all days) was visualized using heatmaps on a $\log_{10}$ scale at 4-minute intervals. Heatmaps were annotated with $PM_{2.5}$ hotspots that cover times greater than a 2-minute period.

K-means clustering was employed to identify clusters of air pollution. The number of clusters (2 for all pollutants) were identified through a variance-by-number-of-cluster plots, where a bend in the plot indicate that a suitable number of clusters are defined to explain the data.

Results and Discussion

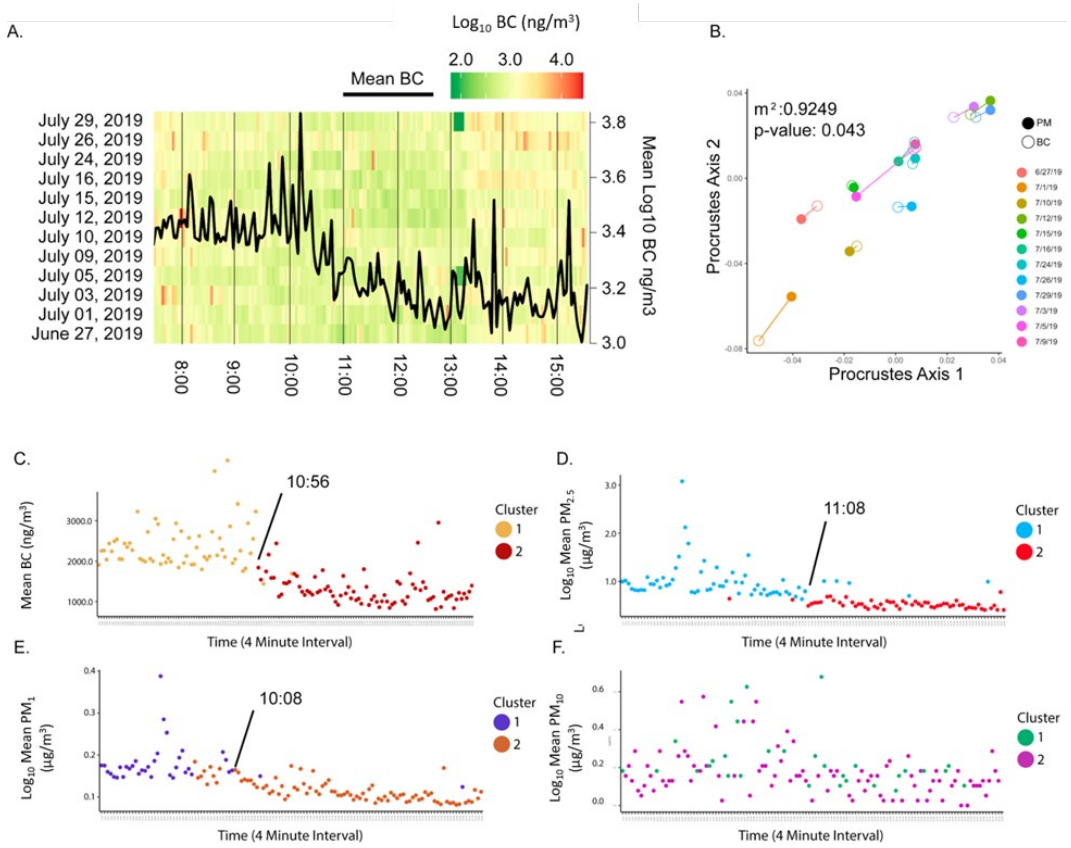

Figure 2. (A) Heatmap showing the $\log_{10}$ concentration of BC across time (x-axis) and different days (y-axis). The black line reflects the $\log_{10}$ mean concentration of BC averaged across all days. (B) Procrustes rotation ordination of correlation between BC and $PM_{2.5}$ on all days with correlation coefficient (m^2) and a p-value. (C) Plot of $\log_{10}$ mean BC concentration over time, colored by cluster, determined by k-means clustering. (D) Plot of $\log_{10}$ mean $PM_{2.5}$ concentration over time, colored by cluster, determined by k-means clustering. (E) Plot of $\log_{10}$ mean PM_1 concentration over time, colored by cluster, determined by k-means clustering. (F) Plot of $\log_{10}$ mean PM_{10} concentration over time, colored by cluster, determined by k-means clustering.

Observed PM and BC concentrations had roughly Poisson distributions, (Figure 3A-D) as lower concentrations were observed much more frequently than higher concentrations. The mean concentrations observed throughout the measurement period were 11.25 ± 5.43 ug/m^3 for PM_1, 11.08 ± 6.25 ug/m^3 for $PM_{2.5}$, 15.57 ± 8.51 ug/m^3 for PM_{10}, and 1.27 ± 0.80 µg/m^3 for BC. The mean $PM_{2.5}$ concentration over the sampling period is slightly greater than, but not significantly different from, the 2018 annual mean $PM_{2.5}$ concentrations found at seven EPA $PM_{2.5}$ monitoring stations in Philadelphia, which ranged from 8.0 – 9.8 µg/m^3 [28]. Variability in PM_{10} concentrations seems to be largely influenced by variation in finer PM concentrations; we find that $PM_{2.5}$ comprises approximately 71% of the observed PM_{10} in Philadelphia. These results are similar to the findings of a previous study on air pollution in Philadelphia, where $PM_{2.5}$ made up 75% of the PM_{10} in the city[29]. Overall, BC accounts for 11.4% of the observed $PM_{2.5}$ in Philadelphia. The ratio of BC / $PM_{2.5}$ in Philadelphia is comparable to the BC / $PM_{2.5}$ ratios of other large cities, which range from 5% - 20%[30]. Pairwise comparison of BC and $PM_{2.5}$ concentrations revealed that the relationship between the two pollutants was generally variable from day to day (Table S4). BC was strongly correlated with $PM_{2.5}$ concentrations at the multivariate level when taking into account their relationships across all days (Figure 3B, Procrustes, $m^2 = 0.9249$, $p = 0.043$), and significant ($p < 0.05$) positive correlations between BC and $PM_{2.5}$ were observed on 10 of the 12 days of data collection (Figure S2). Among days where we found a significant correlation between $PM_{2.5}$ and BC, weak to moderate relationships were observed (Figure SI-2, Spearman's ρ: 0.215-0.616); variation in this relationship from day to day is due in part to the heterogeneity of emission sources and the urban landscape[23]. The high

192 $PM_{2.5}$ / PM_{10} ratio and abundance of BC in Philadelphia are indicative of the significant impact

193 that traffic-related emissions have on air pollution concentrations throughout Philadelphia[31–33].

Spatial Variation

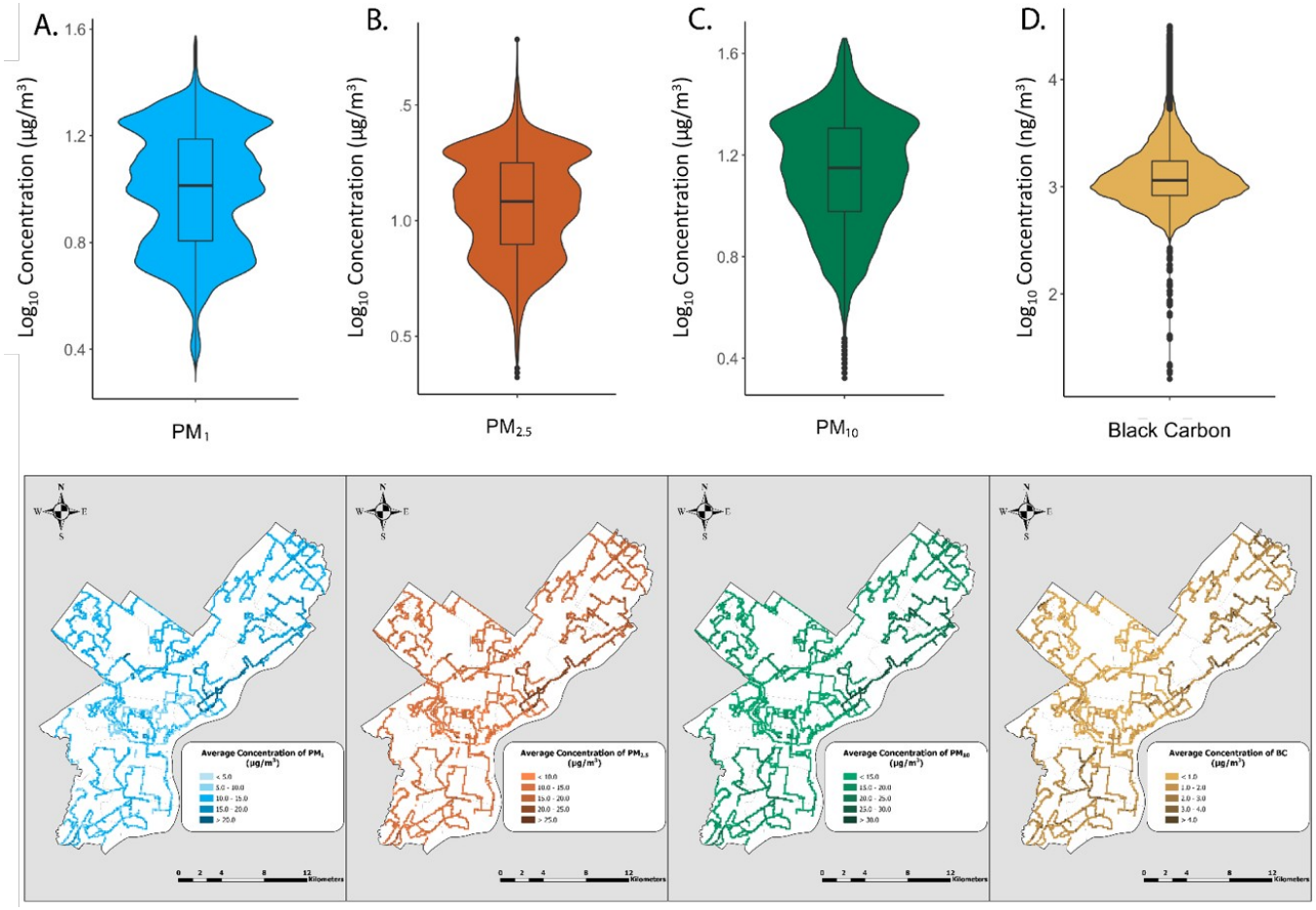

Figure 3. Violin plots and maps for (A) PM_1, (B) $PM_{2.5}$, (C) PM_{10}, and (D) BC. Violin plots show the distribution of all observed air pollutant concentrations on a log_{10} scale, while maps show the overall average concentration of each pollutant in each 120 m^2 cell sampled over the data collection period.

We found that PM_1, $PM_{2.5}$, and PM_{10} have a similar spatial distribution throughout Philadelphia (Figure 3). Similarities between the PM_{10} and the $PM_{2.5}$ and PM_1 distributions indicate that finer PM constitutes a significant proportion of Philadelphia's PM and thus drives a majority of the variation in PM_{10} concentrations. The lowest concentrations of PM and BC in Philadelphia were generally found in Philadelphia's Lower North (LNO), West Park (WP), and West (W) planning zones. The highest concentrations of PM across all size fractions were found in Philadelphia's North Delaware (NDEL), River Wards (RW), and North (NOR) planning zones. RW contains a port and large public utility properties, as well as other industries, which may be significant sources of PM in this area[34]. Interestingly, BC concentrations vary considerably in these planning zones, which suggests that traffic-related emissions do not contribute as much to the ambient air pollution in these particular areas relative to other sources. BC concentrations are highest in the RW, Lower Far Northeast (LFNR), and Upper Far Northeast (UFNE) planning zones. It is possible that increased traffic-related emissions resulting from the proximity of these zones to Interstate 95 may be the cause of high BC concentrations in this region. The Northeast Philadelphia Airport in RFNE, where BC concentrations are elevated, may also contribute significantly to BC emissions; landings and takeoffs by aircrafts at airports, have been shown to increase local BC concentrations in the atmosphere[35].

Statistically significant hotspots were found on all days across all measured size fractions of PM and BC throughout Philadelphia. The average concentrations of hotspots (Figure 4) within a given cell ranged from 8.7 ± 4.6 μg/m^3 for BC; 18.7 ± 7.1 μg/m^3 for PM_1; 28.0 ± 8.8 μg/m^3 for $PM_{2.5}$; and 46.0 ± 17.3 μg/m^3 for $PM_{10.}$ While there is slight variation in the location of hotspots among the different pollutants, the overall spatial distribution of hotspots throughout

Philadelphia is similar across all PM size fractions and BC (Figure 4). Relatively few hotspots were found in northern and western Philadelphia, which are located well outside of Philadelphia's urban core. In these areas, traffic-related emissions are likely not as prominent as in the urban core, and a greater abundance of vegetation may attenuate air pollution primarily by uptake via leaf stomata and particle deposition[36,37]. Each pollutant had hotspots that exhibited a tendency to recur in the same locations across multiple days; hotspots for PM_1 appeared in the same cell on as many as six separate days throughout the data collection period, while hotspots for $PM_{2.5}$, PM_{10}, and BC appeared in the same cell on up to five different days. The recurrence of hotspots in specific locations suggests that there are areas in Philadelphia where pollutant concentrations are constantly elevated relative to the surrounding area. A notable cluster of cells in the NDEL, RW, and NOR planning zones contain high concentration PM hotspots across multiple days. Other clusters of recurring hotspots are found within the University Southwest (USW) and LFNE planning zones.

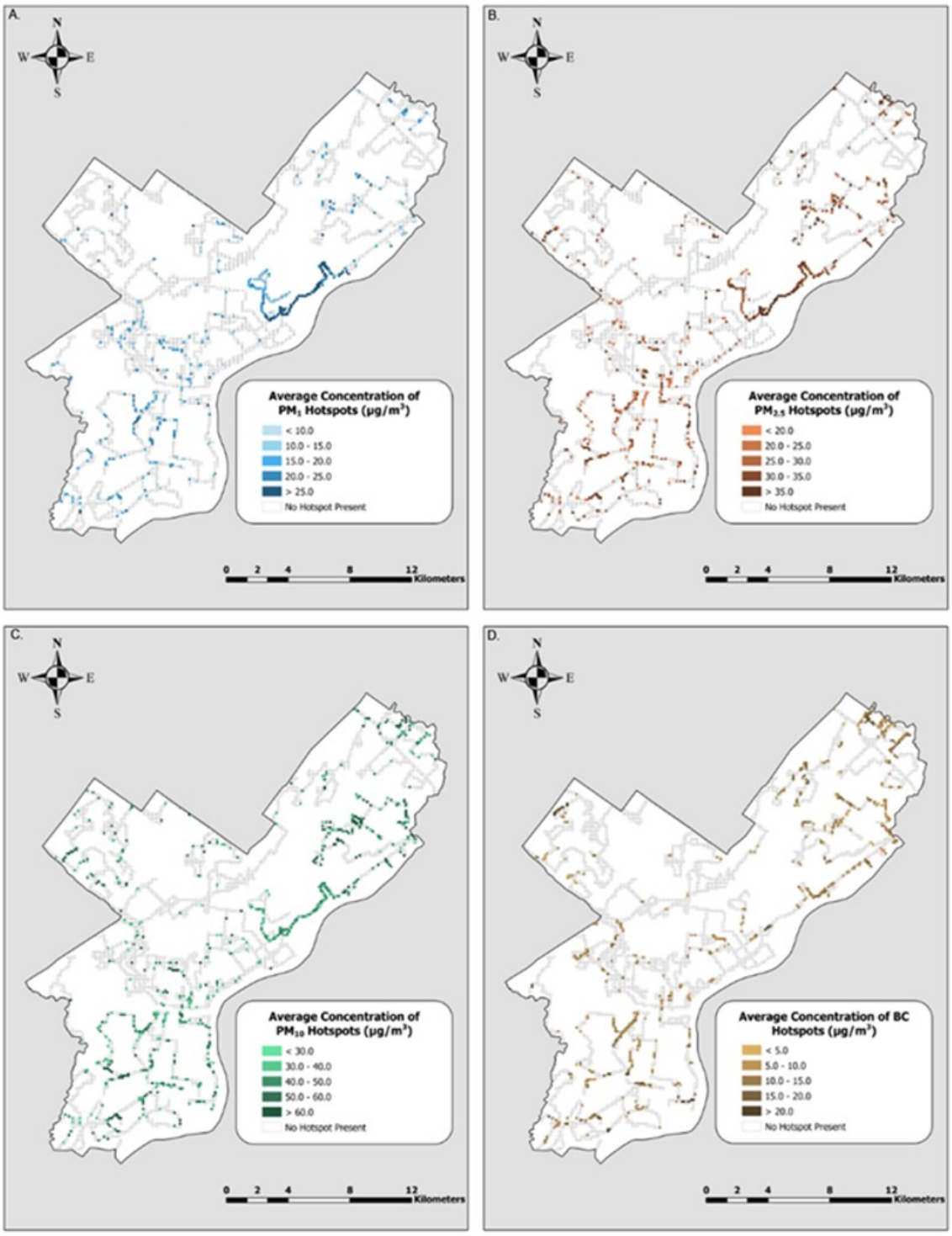

Figure 4. Maps displaying the locations and average concentrations of hotspots for (A) PM_1, (B) $PM_{2.5}$, (C) PM_{10}, and (D) BC in Philadelphia.

Temporal Variation

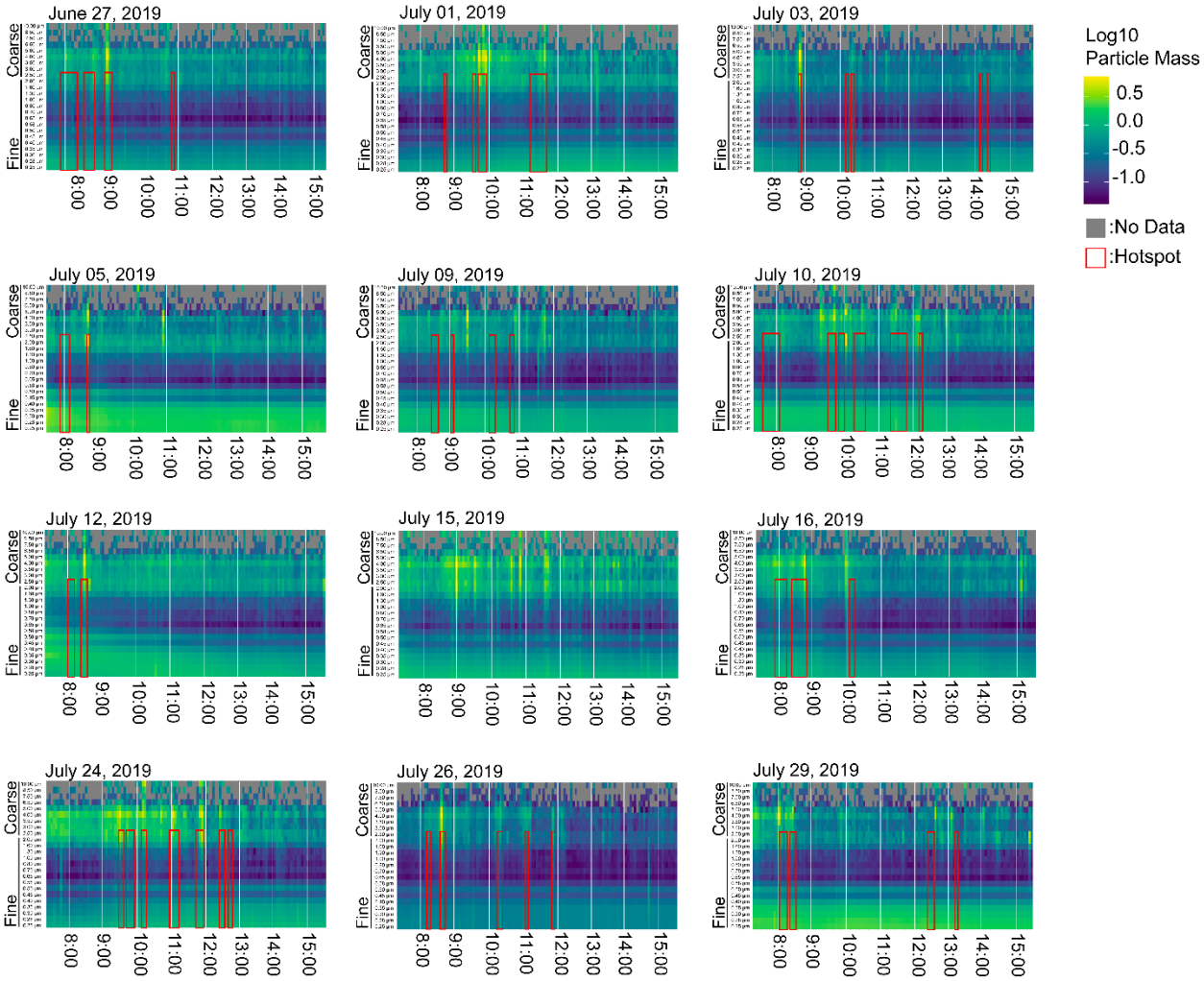

Figure 4. Heatmap of $\log_{10}$ PM mass values across 24 fine and coarse size fractions throughout each day of data collection. Time of day is denoted on the x-axis. Hotspots for $PM_{2.5}$ fraction covering > 2 minute periods are identified by vertical red boxes. July 15, 2019 was excluded from hotspot analysis; as such, no hotspots are identified.

PM emissions were not uniform across all size fractions measured. All observations indicate the presence of particulate matter of 5 µm in diameter or smaller. PM exceeding 5 µm in diameter is not as ubiquitous throughout the data collection period, with larger particles not being detected at times throughout each day. Mass values observed for particles 1.6 µm diameter and larger generally demonstrated the greatest variation throughout each day, with

252 particles with a diameter 0.5 µm and smaller also showing less within-day variation (Figure 4).
253 Trends emerged despite significant temporal variation in the concentration and distribution of
254 PM_1, $PM_{2.5}$, and PM_{10} ($p < 0.05$, Tables SI-1 – SI-3). The $PM_{2.5}$ size fraction (Figure 2D) clustered
255 into two distinct time periods separated at approximately 11:08 AM, which complements our
256 finding of BC clusters at approximately 10:56 AM (Figure 2C). While this relationship is expected
257 due to BC largely contributing to $PM_{2.5}$ composition in urban areas from vehicles[38], larger (PM_{10})
258 and smaller size (PM_1) fractions varied in their separation of peaks by time. PM_1 displayed less
259 discrete temporal clustering (Figure 2E), with a break in clustering at approximately 10:08 AM.
260 A cutoff was not found for PM_{10}. The lack of temporal clustering for PM_{10}, as seen in a previous
261 mobile monitoring study[39], affirms that larger particulate matter emission is stochastic across
262 the urban landscape, and may be attributed to crustal sources (e.g. dust resuspension). These
263 results complement findings in other mobile monitoring studies where PM size fractions exhibit
264 different concentrations in the morning and afternoon[40].

265 The number, duration, and timing of $PM_{2.5}$ hotspots (Figure 4) varied from day to day;
266 however, they were most consistently seen from 8:00 – 9:00 AM (30.19% of all hotspots) in
267 complement with other studies[41,42]. These hotspots are likely attributed to primary particles
268 emitted from morning rush-hour traffic, where the number and density of vehicles on the road
269 is high relative to the rest of the day. The presence of hotspots outside the morning trend may
270 be attributed to areas closer to industrial sites, such as those located along the I-676 and I-95
271 corridors[43]. While a substantial fraction of the $PM_{2.5}$ in urban areas originates from combustion
272 engines, increased solar radiation during the summer months likely enhances the contribution
273 of secondary particles formed from photooxidation of precursor molecules[44].

In this study, we demonstrate the potential for a mobile monitoring approach to examine fine-scale spatiotemporal distribution of air pollutants in a major city. Our findings demonstrate the variability of PM and BC concentrations in space and time and indicate that trends in variation are dependent on the size and type of pollutant. Our analysis is limited by relatively few repetitions of routes and variability in the accuracy of geolocation data. As our sampling occurs entirely on Philadelphia roadways, it should be noted that our measurements may be slightly different relative to ambient air further from roads. While urban air pollution near roadways tends to be higher due to the influence of traffic-related emissions[45–47], a 2017 study of air pollution along pedestrian walkways in Philadelphia observed higher average pollutant concentrations than those observed in this study[6]. More extensive sampling would allow for additional confidence in observed trends and provide opportunities to observe air pollution patterns at other temporal scales; sampling during late afternoon and evening hours would provide additional insight into air pollution trends throughout the day, while increased repetition of measurements both within and across seasons would allow for a seasonal analysis of air pollution trends[48]. Hot spot analysis reveals regions in Philadelphia that merit further study, especially in the context of vulnerable and socioeconomically disadvantaged populations that may be disproportionately impacted by air pollution.

Though our analysis reveals spatiotemporal variation in PM and BC and possible causes of this variation, it stops short of estimating the contributions of specific sources to variability; as our air pollution measurements covary in space and time, it is difficult to quantify the extent of variation resulting from spatial influences (locations of point sources, movement of non-point sources) and temporal influences (temporally-sensitive atmospheric processes, random

events) separately. Future analyses should focus on the influence of urban structure on air pollution. Cities can be quite different from one another compositionally and structurally, and the roles of urban structure[49] and land use[6,50] may be important drivers of variation in urban air pollution. This analysis can be used to help identify general times and places across urban environments where air pollution may have the greatest adverse impacts on human and environmental health, which is paramount to effective air pollution mitigation and reduction of negative health impacts associated with air pollution.

Acknowledgements:

We would like to thank Meghan Conway and Alexander Saad for their assistance in data collection. Financial support for this study was provided through National Science Foundation (NSF) grant #1832407.

Conflicts of Interest:

The authors declare no conflicts of interest.

Supporting Information:

Supporting Information includes:

- Maps showing variation in the route travels (Figure SI-1)
- Spearman correlation tests of BC and $PM_{2.5}$ (Figure SI-2)
- Pairwise Mann-Whitney U-tests comparing pollutant observations between days (Tables SI-1 – 4)

References:

(1) Pulmonary Health Effects of Air Pollution https://www.ncbi.nlm.nih.gov/pmc/articles/PMC4776742/ (accessed Jun 29, 2020).

(2) Strosnider, H.; Kennedy, C.; Monti, M.; Yip, F. Rural and Urban Differences in Air Quality, 2008-2012, and Community Drinking Water Quality, 2010-2015 - United States. *MMWR Surveillance Summaries* **2017**, *66* (13), 2010–2015. https://doi.org/10.15585/mmwr.ss6613a1.

(3) World Population Projected to Reach 9.7 Billion by 2050 | UN DESA | United Nations Department of Economic and Social Affairs.

(4) Tsapakis, M.; Lagoudaki, E.; Stephanou, E. G.; Kavouras, I. G.; Koutrakis, P.; Oyola, P.; von Baer, D. The Composition and Sources of PM2.5 Organic Aerosol in Two Urban Areas of Chile. *Atmospheric Environment* **2002**, *36* (23), 3851–3863. https://doi.org/10.1016/S1352-2310(02)00269-8.

(5) Kelly, F. J.; Fussell, J. C. Size, Source and Chemical Composition as Determinants of Toxicity Attributable to Ambient Particulate Matter. *Atmospheric Environment* **2012**, *60*, 504–526. https://doi.org/10.1016/j.atmosenv.2012.06.039.

(6) Shakya, K. M.; Kremer, P.; Henderson, K.; McMahon, M.; Peltier, R. E.; Bromberg, S.; Stewart, J. Mobile Monitoring of Air and Noise Pollution in Philadelphia Neighborhoods during Summer 2017. *Environ. Pollut.* **2019**, *255* (Pt 1), 113195–113195. https://doi.org/10.1016/j.envpol.2019.113195.

(7) US EPA, O. *Report on the Environment (ROE)*; Collections and Lists; 2015.

(8) Hotspots of black carbon and PM2.5 in an urban area and relationships to traffic characteristics - ScienceDirect https://www.sciencedirect.com/science/article/pii/S0269749116305978 (accessed Jun 29, 2020).

(9) Dominici, F.; Peng, R. D.; Bell, M. L.; Pham, L.; McDermott, A.; Zeger, S. L.; Samet, J. M. Fine Particulate Air Pollution and Hospital Admission for Cardiovascular and Respiratory Diseases. *JAMA* **2006**, *295* (10), 1127–1134. https://doi.org/10.1001/jama.295.10.1127.

(10) Dockery, D. W.; Pope, C. A.; Xu, X.; Spengler, J. D.; Ware, J. H.; Fay, M. E.; Ferris, B. G.; Speizer, F. E. An Association between Air Pollution and Mortality in Six U.S. Cities. *New England Journal of Medicine* **1993**, *329* (24), 1753–1759. https://doi.org/10.1056/NEJM199312093292401.

(11) Miller, F. J.; Gardner, D. E.; Graham, J. A.; Jr, R. E. L.; Wilson, W. E.; Bachmann, J. D. Size Considerations for Establishing a Standard for Inhalable Particles. *Journal of the Air Pollution Control Association* **1979**, *29* (6), 610–615. https://doi.org/10.1080/00022470.1979.10470831.

(12) Shakya, K. M.; Rupakheti, M.; Aryal, K.; Peltier, R. E. Respiratory Effects of High Levels of Particulate Exposure in a Cohort of Traffic Police in Kathmandu, Nepal: *Journal of Occupational and Environmental Medicine* **2016**, *58* (6), e218–e225. https://doi.org/10.1097/JOM.0000000000000753.

(13) Rabinovitch, N.; Strand, M.; Gelfand, E. W. Particulate Levels Are Associated with Early Asthma Worsening in Children with Persistent Disease. *Am. J. Respir. Crit. Care Med.* **2006**, *173* (10), 1098–1105. https://doi.org/10.1164/rccm.200509-1393OC.

(14) Paul, G.; Nolen, J. E.; Alexander, L.; Bender, L. K.; Vleet, V.; Barrett, W.; Jump, Z.; Rappaport, S.; Samet, J. M.; Ballentine, N.; Nimirowski, T.; Innocenzi, L.; Wojs, V.; Lavelle, L.; Clark, C.; Fitzgerald, J.; Eyer, A.; Lacina, K.; Macmunn, A.; Tubbs, G.; Meyer, E.; Albiero, M.; Montague, S.; Finstad, C.; Boucher, L.; Martin, V.; Consulting, B. R.; Designs, O. State of the Air 2019. **2019**.

(15) Cao, C.; Jiang, W.; Wang, B.; Fang, J.; Lang, J.; Tian, G.; Jiang, J.; Zhu, T. F. Inhalable Microorganisms in Beijing's PM 2.5 and PM 10 Pollutants during a Severe Smog Event. *Appl. Environ. Microbiol.* **2014**. https://doi.org/10.1021/es4048472.

(16) Zhang, Y.-L.; Cao, F. Fine Particulate Matter (PM 2.5) in China at a City Level. *Scientific Reports* **2015**, *5* (1), 14884. https://doi.org/10.1038/srep14884.
(17) Vallius, M.; Janssen, N. A. H.; Heinrich, J.; Hoek, G.; Ruuskanen, J.; Cyrys, J.; Van Grieken, R.; de Hartog, J. J.; Kreyling, W. G.; Pekkanen, J. Sources and Elemental Composition of Ambient PM2.5 in Three European Cities. *Science of The Total Environment* **2005**, *337* (1), 147–162. https://doi.org/10.1016/j.scitotenv.2004.06.018.
(18) Zhang, A.; Qi, Q.; Jiang, L.; Zhou, F.; Wang, J. Population Exposure to PM2.5 in the Urban Area of Beijing. *PLOS ONE* **2013**, *8* (5), e63486. https://doi.org/10.1371/journal.pone.0063486.
(19) A population exposure model for particulate matter: case study results for PM 2.5 in Philadelphia, PA | Journal of Exposure Science & Environmental Epidemiology https://www.nature.com/articles/7500188 (accessed Jul 24, 2020).
(20) Van Poppel, M.; Peters, J.; Bleux, N. Methodology for Setup and Data Processing of Mobile Air Quality Measurements to Assess the Spatial Variability of Concentrations in Urban Environments. *Environmental Pollution* **2013**, *183*, 224–233. https://doi.org/10.1016/j.envpol.2013.02.020.
(21) Deville Cavellin, L.; Weichenthal, S.; Tack, R.; Ragettli, M. S.; Smargiassi, A.; Hatzopoulou, M. Investigating the Use Of Portable Air Pollution Sensors to Capture the Spatial Variability Of Traffic-Related Air Pollution. *Environ. Sci. Technol.* **2016**, *50* (1), 313–320. https://doi.org/10.1021/acs.est.5b04235.
(22) Targino, A. C.; Rodrigues, M. V. C.; Krecl, P.; Cipoli, Y. A.; Ribeiro, J. P. M. Commuter Exposure to Black Carbon Particles on Diesel Buses, on Bicycles and on Foot: A Case Study in a Brazilian City. *Environmental Science and Pollution Research* **2018**, *25* (2), 1132–1146. https://doi.org/10.1007/s11356-017-0517-x.
(23) Van den Bossche, J.; Peters, J.; Verwaeren, J.; Botteldooren, D.; Theunis, J.; De Baets, B. Mobile Monitoring for Mapping Spatial Variation in Urban Air Quality: Development and Validation of a Methodology Based on an Extensive Dataset. *Atmospheric Environment* **2015**, *105*, 148–161. https://doi.org/10.1016/j.atmosenv.2015.01.017.
(24) Gozzi, F.; Della Ventura, G.; Marcelli, A. Mobile Monitoring of Particulate Matter: State of Art and Perspectives. *Atmospheric Pollution Research* **2016**, *7* (2), 228–234. https://doi.org/10.1016/j.apr.2015.09.007.
(25) Hamstead, Z. A.; Kremer, P.; Larondelle, N.; McPhearson, T.; Haase, D. Classification of the Heterogeneous Structure of Urban Landscapes (STURLA) as an Indicator of Landscape Function Applied to Surface Temperature in New York City. *Ecological Indicators* **2016**, *70*, 574–585. https://doi.org/10.1016/j.ecolind.2015.10.014.
(26) Stewart, J. D.; Kremer, P.; Shakya, K. M.; Conway, M.; Saad, A. Outdoor Atmospheric Microbial Diversity Is Associated with Three-Dimensional Urban Landscape Structure and Differs from Indoor-Transit Systems. *bioRxiv* **2020**, 2020.06.17.157651. https://doi.org/10.1101/2020.06.17.157651.
(27) Getis, A.; Ord, J. K. The Analysis of Spatial Association by Use of Distance Statistics. *Geographical Analysis* **1992**, *24* (3), 189–206. https://doi.org/10.1111/j.1538-4632.1992.tb00261.x.
(28) City of Philadelphia, Department of Public Health, Air Management Services. *Philadelphia's Air Quality Report 2018*; 2019.
(29) Burton, R. M.; Suh, H. H.; Koutrakis, P. Spatial Variation in Particulate Concentrations within Metropolitan Philadelphia. *Environmental Science and Technology* **1996**, *30* (2), 400–407. https://doi.org/10.1021/es950030f.
(30) Yu, N.; Zhu, Y.; Xie, X.; Yan, C.; Zhu, T.; Zheng, M. Characterization of Ultrafine Particles and Other Traffic Related Pollutants near Roadways in Beijing. *Aerosol and Air Quality Research* **2015**, *15*. https://doi.org/10.4209/aaqr.2014.11.0295.

(31) Spatial and Temporal Variability of the PM2.5/PM10 Ratio in Wuhan, Central China - Aerosol and Air Quality Research https://aaqr.org/articles/aaqr-16-09-oa-0406 (accessed Jun 29, 2020).
(32) Ni, M.; Huang, J.; Lu, S.; Li, X.; Yan, J.; Cen, K. A Review on Black Carbon Emissions, Worldwide and in China. *Chemosphere* **2014**, *107*, 83–93. https://doi.org/10.1016/j.chemosphere.2014.02.052.
(33) Kim, S.; Yu, S.; Yun, D. Spatiotemporal Association of Real-Time Concentrations of Black Carbon (BC) with Fine Particulate Matters (PM2.5) in Urban Hotspots of South Korea. *International Journal of Environmental Research and Public Health* **2017**, *14* (11), 1350. https://doi.org/10.3390/ijerph14111350.
(34) Philadelphia City Planning Commission. *Philadelphia2035*.
(35) Agarwal, A.; Speth, R. L.; Fritz, T. M.; Jacob, S. D.; Rindlisbacher, T.; Iovinelli, R.; Owen, B.; Miake-Lye, R. C.; Sabnis, J. S.; Barrett, S. R. H. SCOPE11 Method for Estimating Aircraft Black Carbon Mass and Particle Number Emissions. *Environ. Sci. Technol.* **2019**, *53* (3), 1364–1373. https://doi.org/10.1021/acs.est.8b04060.
(36) Beckett, K. P.; Freer-Smith, P. H.; Taylor, G. The Capture of Particulate Pollution by Trees at Five Contrasting Urban Sites. *Arboricultural Journal* **2000**, *24* (2–3), 209–230. https://doi.org/10.1080/03071375.2000.9747273.
(37) Nowak, D. J.; Crane, D. E.; Stevens, J. C. Air Pollution Removal by Urban Trees and Shrubs in the United States. *Urban Forestry & Urban Greening* **2006**, *4* (3), 115–123. https://doi.org/10.1016/j.ufug.2006.01.007.
(38) Ježek, I.; Katrašnik, T.; Westerdahl, D.; Močnik, G. Black Carbon, Particle Number Concentration and Nitrogen Oxide Emission Factors of Random in-Use Vehicles Measured with the on-Road Chasing Method. *Atmospheric Chemistry and Physics* **2015**, *15* (19), 11011–11026. https://doi.org/10.5194/acp-15-11011-2015.
(39) Peters, J.; Theunis, J.; Poppel, M. V.; Berghmans, P. Monitoring PM10 and Ultrafine Particles in Urban Environments Using Mobile Measurements. *Aerosol Air Qual. Res.* **2013**, *13* (2), 509–522. https://doi.org/10.4209/aaqr.2012.06.0152.
(40) Hankey, S.; Marshall, J. D. On-Bicycle Exposure to Particulate Air Pollution: Particle Number, Black Carbon, PM2.5, and Particle Size. *Atmospheric Environment* **2015**, *122*, 65–73. https://doi.org/10.1016/j.atmosenv.2015.09.025.
(41) Tunno, B. J.; Shields, K. N.; Lioy, P.; Chu, N.; Kadane, J. B.; Parmanto, B.; Pramana, G.; Zora, J.; Davidson, C.; Holguin, F.; Clougherty, J. E. Understanding Intra-Neighborhood Patterns in PM2.5 and PM10 Using Mobile Monitoring in Braddock, PA. *Environ Health* **2012**, *11* (1), 76. https://doi.org/10.1186/1476-069X-11-76.
(42) Zhao, X.; Zhang, X.; Xu, X.; Xu, J.; Meng, W.; Pu, W. Seasonal and Diurnal Variations of Ambient PM2.5 Concentration in Urban and Rural Environments in Beijing. *Atmospheric Environment* **2009**, *43* (18), 2893–2900. https://doi.org/10.1016/j.atmosenv.2009.03.009.
(43) Chow, J. C.; Watson, J. G.; Fujita, E. M.; Lu, Z.; Lawson, D. R.; Ashbaugh, L. L. Temporal and Spatial Variations of PM2.5 and PM10 Aerosol in the Southern California Air Quality Study. *Atmospheric Environment* **1994**, *28* (12), 2061–2080. https://doi.org/10.1016/1352-2310(94)90474-X.
(44) Claeys, M.; Graham, B.; Vas, G.; Wang, W.; Vermeylen, R.; Pashynska, V.; Cafmeyer, J.; Guyon, P.; Andreae, M. O.; Artaxo, P.; Maenhaut, W. Formation of Secondary Organic Aerosols Through Photooxidation of Isoprene. *Science* **2004**, *303* (5661), 1173–1176. https://doi.org/10.1126/science.1092805.
(45) Barzyk, T. M.; George, B. J.; Vette, A. F.; Williams, R. W.; Croghan, C. W.; Stevens, C. D. Development of a Distance-to-Roadway Proximity Metric to Compare near-Road Pollutant Levels to a Central Site Monitor. *Atmospheric Environment* **2009**, *43* (4), 787–797. https://doi.org/10.1016/j.atmosenv.2008.11.002.

(46) Yu, C. H.; Fan, Z.; Lioy, P. J.; Baptista, A.; Greenberg, M.; Laumbach, R. J. A Novel Mobile Monitoring Approach to Characterize Spatial and Temporal Variation in Traffic-Related Air Pollutants in an Urban Community. *Atmospheric Environment* **2016**, *141*, 161–173. https://doi.org/10.1016/j.atmosenv.2016.06.044.
(47) Karner, A. A.; Eisinger, D. S.; Niemeier, D. A. Near-Roadway Air Quality: Synthesizing the Findings from Real-World Data. *Environ. Sci. Technol.* **2010**, *44* (14), 5334–5344. https://doi.org/10.1021/es100008x.
(48) Liu, Y.; Wu, J.; Yu, D.; Ma, Q. The Relationship between Urban Form and Air Pollution Depends on Seasonality and City Size. *Environ Sci Pollut Res* **2018**, *25* (16), 15554–15567. https://doi.org/10.1007/s11356-018-1743-6.
(49) Cárdenas Rodríguez, M.; Dupont-Courtade, L.; Oueslati, W. Air Pollution and Urban Structure Linkages: Evidence from European Cities. *Renewable and Sustainable Energy Reviews* **2016**, *53*, 1–9. https://doi.org/10.1016/j.rser.2015.07.190.
(50) Weng, Q.; Yang, S. Urban Air Pollution Patterns, Land Use, and Thermal Landscape: An Examination of the Linkage Using GIS. *Environ Monit Assess* **2006**, *117* (1), 463–489. https://doi.org/10.1007/s10661-006-0888-9.

Supplemental

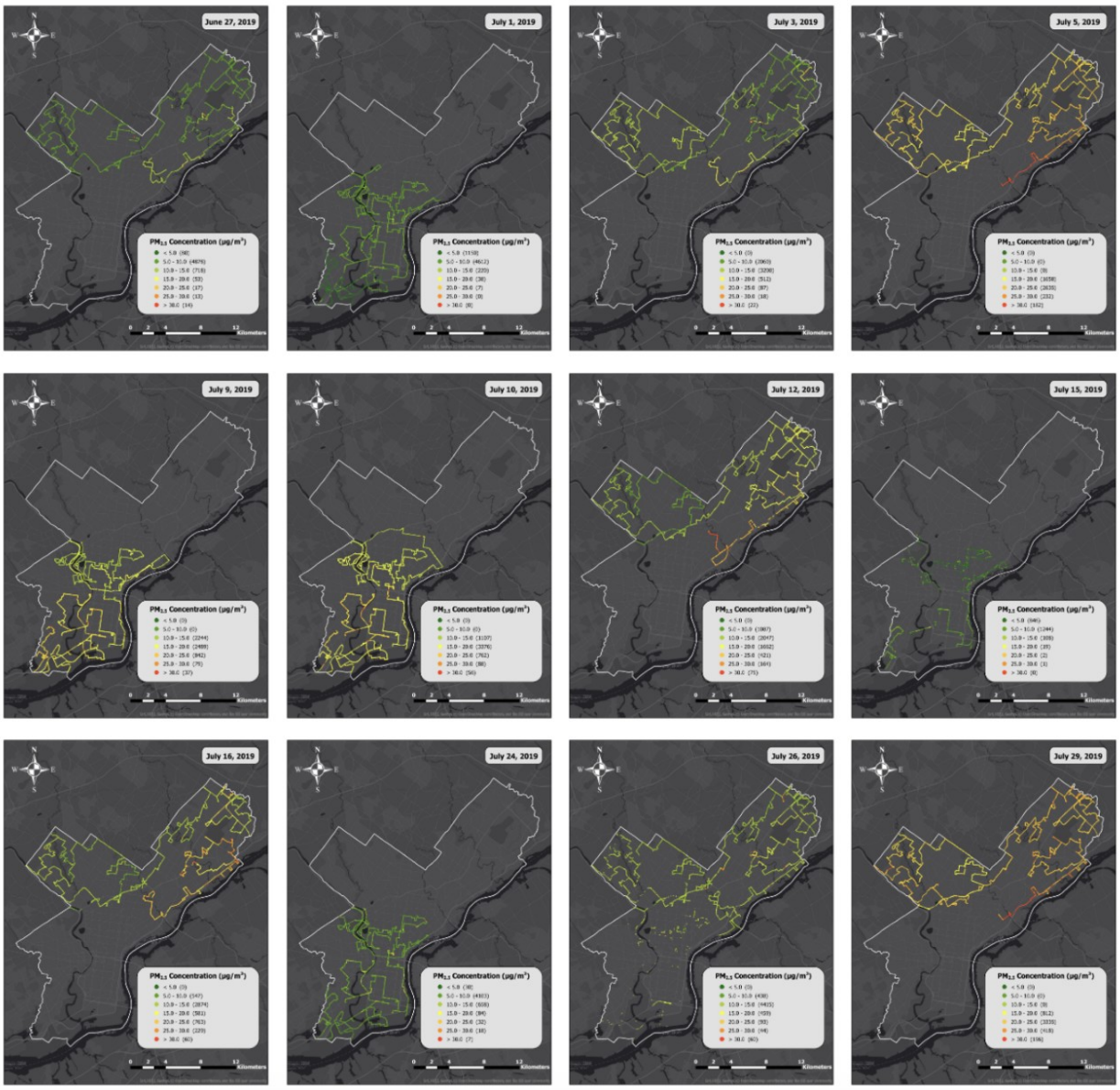

476

477 Figure SI-1. Maps showing all $PM_{2.5}$ observations on each day of data collection. As a result of
478 intermittent road closures, the routes traveled on each day vary slightly.

479

480

481

482

483

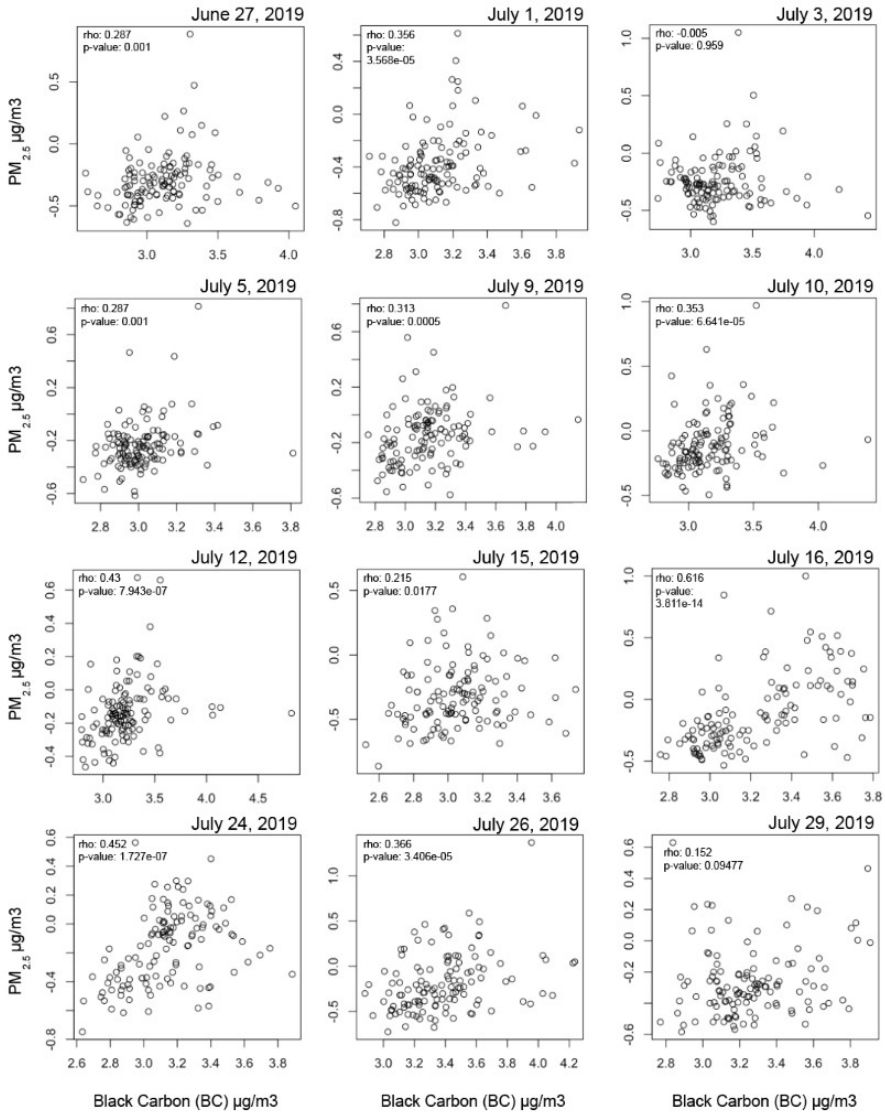

Figure SI-2. Spearman correlations of BC and $PM_{2.5}$ concentrations on each day, with correlation coefficient (ρ) and p-value at the top left of each subplot.

Table SI-1: Pairwise Mann-Whitney U tests with Bonferroni correction for concentrations of PM_1.

Date	6/27/19	7/1/19	7/3/19	7/5/19	7/9/19	7/10/19	7/12/19	7/15/19	7/16/19	7/24/19	7/26/19
6/27/19	0	0	0	0	0	0	0	0	0	0	0
7/1/19	2.20E-16	0	0	0	0	0	0	0	0	0	0
7/3/19	2.20E-16	2.20E-16	0	0	0	0	0	0	0	0	0
7/5/19	2.20E-16	2.20E-16	2.20E-16	0	0	0	0	0	0	0	0
7/9/19	2.20E-16	2.20E-16	2.20E-16	2.20E-16	0	0	0	0	0	0	0
7/10/19	2.20E-16	2.20E-16	2.20E-16	2.20E-16	2.20E-16	0	0	0	0	0	0
7/12/19	2.20E-16	2.20E-16	2.20E-16	2.20E-16	2.20E-16	2.20E-16	0	0	0	0	0
7/15/19	2.20E-16	2.20E-16	2.20E-16	2.20E-16	2.20E-16	2.20E-16	2.20E-16	0	0	0	0
7/16/19	2.20E-16	2.20E-16	2.20E-16	2.20E-16	2.20E-16	2.20E-16	6.00E-14	2.20E-16	0	0	0
7/24/19	2.20E-16	2.20E-16	2.20E-16	2.20E-16	2.20E-16	2.20E-16	2.20E-16	2.20E-16	2.20E-16	0	0
7/26/19	2.20E-16	2.20E-16	2.20E-16	2.20E-16	2.20E-16	2.20E-16	2.20E-16	2.20E-16	2.20E-16	2.20E-16	0
7/29/19	2.20E-16	2.20E-16	2.20E-16	2.20E-16	2.20E-16	2.20E-16	2.20E-16	2.20E-16	2.20E-16	2.20E-16	2.20E-16

Table SI-2: Pairwise Mann-Whitney U tests with Bonferroni correction for concentrations of $PM_{2.5}$.

Date	6/27/19	7/1/19	7/10/19	7/12/19	7/15/19	7/16/19	7/24/19	7/26/19	7/29/19	7/3/19	7/5/19
6/27/19	0	0	0	0	0	0	0	0	0	0	0
7/1/19	6.60E-270	0	0	0	0	0	0	0	0	0	0
7/10/19	2.20E-16	2.20E-16	0	0	0	0	0	0	0	0	0
7/12/19	2.20E-16	2.20E-16	2.20E-16	0	0	0	0	0	0	0	0
7/15/19	2.20E-16	1.98E-10	2.20E-16	2.20E-16	0	0	0	0	0	0	0
7/16/19	2.20E-16	2.20E-16	2.20E-16	1.41E-10	2.20E-16	0	0	0	0	0	0
7/24/19	1.90E-120	2.20E-16	2.20E-16	2.20E-16	2.20E-16	2.20E-16	0	0	0	0	0
7/26/19	2.20E-16	2.20E-16	2.20E-16	1.91E-23	2.20E-16	1.12E-87	2.20E-16	0	0	0	0
7/29/19	2.20E-16	2.20E-16	2.20E-16	2.20E-16	2.20E-16	2.20E-16	2.20E-16	2.20E-16	0	0	0
7/3/19	2.20E-16	2.20E-16	2.20E-16	1.45E-71	2.20E-16	6.32E-157	2.20E-16	3.82E-20	2.20E-16	0	0
7/5/19	2.20E-16	2.20E-16	2.20E-16	2.20E-16	2.20E-16	2.20E-16	2.20E-16	2.20E-16	1.07E-72	2.20E-16	0
7/9/19	2.20E-16	2.20E-16	6.19E-14	2.20E-16	2.20E-16	2.20E-16	2.20E-16	2.20E-16	2.20E-16	2.20E-16	2.20E-16

Table SI-3: Pairwise Mann-Whitney U tests with Bonferroni correction for concentrations of PM_{10}.

Date	6/27/19	7/1/19	7/10/19	7/12/19	7/15/19	7/16/19	7/24/19	7/26/19	7/29/19	7/3/19	7/5/19
6/27/19	0	0	0	0	0	0	0	0	0	0	0
7/1/19	2.20E-16	0	0	0	0	0	0	0	0	0	0
7/10/19	2.20E-16	2.20E-16	0	0	0	0	0	0	0	0	0
7/12/19	2.20E-16	2.20E-16	2.20E-16	0	0	0	0	0	0	0	0
7/15/19	9.43E-167	1.54E-12	2.20E-16	2.20E-16	0	0	0	0	0	0	0
7/16/19	2.20E-16	2.20E-16	6.07E-211	3.26E-18	2.20E-16	0	0	0	0	0	0
7/24/19	2.64E-62	2.20E-16	2.20E-16	2.20E-16	2.20E-16	2.20E-16	0	0	0	0	0
7/26/19	2.20E-16	2.20E-16	2.20E-16	2.13E-17	2.20E-16	1.43E-79	2.20E-16	0	0	0	0
7/29/19	2.20E-16	2.20E-16	2.20E-16	2.20E-16	2.20E-16	2.20E-16	2.20E-16	2.20E-16	0	0	0
7/3/19	2.20E-16	2.20E-16	2.20E-16	8.51E-103	2.20E-16	4.71E-217	2.20E-16	9.48E-46	2.20E-16	0	0
7/5/19	2.20E-16	2.20E-16	2.20E-16	2.20E-16	2.20E-16	2.20E-16	2.20E-16	2.20E-16	1.17E-54	2.20E-16	0
7/9/19	2.20E-16	2.20E-16	2.40E-10	9.23E-242	2.20E-16	4.87E-150	2.20E-16	2.20E-16	2.20E-16	2.20E-16	2.20E-16

Table SI-4: Pairwise Mann-Whitney U tests with Bonferroni correction for concentrations of BC.

Date	6/27/	7/1/1	7/10/	7/12/	7/15/	7/16/	7/24/	7/26/	7/29/	7/3/1	7/5/1

	19	9	19	19	19	19	19	19	19	9	9
6/27/19	0	0	0	0	0	0	0	0	0	0	0
7/1/19	35.3232	0	0	0	0	0	0	0	0	0	0
7/10/19	0.042016	0.148038	0	0	0	0	0	0	0	0	0
7/12/19	25.674	40.9266	2.47038	0	0	0	0	0	0	0	0
7/15/19	7.8408	1.43616	2.09E-05	0.891	0	0	0	0	0	0	0
7/16/19	0.274692	1.3827	51.5856	3.74946	0.001339	0	0	0	0	0	0
7/24/19	1.79454	4.4913	20.3544	15.4308	0.004103	29.3304	0	0	0	0	0
7/26/19	1.45E-14	1.45E-14	4.8E-09	1E-11	1.45E-14	9.07E-07	4.27E-10	0	0	0	0
7/29/19	7.6E-05	0.000101	1.82028	0.017714	4.26E-09	2.88948	0.280566	0.002312	0	0	0
7/3/19	8.78E-06	7.22E-06	0.67848	0.010501	1.15E-10	0.86328	0.150282	0.000626	60.9048	0	0
7/5/19	24.7038	4.37052	1.51E-05	2.99178	29.8584	0.006712	0.04288	1.45E-14	1.67E-09	2.12E-12	0
7/9/19	0.00351	0.004811	20.3148	0.528726	1.64E-07	17.9454	5.93868	1.47E-07	9.57	8.9958	3.81E-08